Mott Transition in the $A15$ Phase of Cs_3C_{60}: Absence of a Pseudogap and Charge Order

H. Alloul,[1] P. Wzietek,[1] T. Mito,[1] D. Pontiroli,[2] M. Aramini,[3,2] M. Riccò,[2] J. P. Itie,[4] and E. Elkaim[4]
[1]*Laboratoire de Physique des Solides, CNRS, Université Paris-Sud, Université Paris-Saclay, 91405 Orsay, France*
[2]*CNISM and Dipartimento di Fisica, Università di Parma—Via G.P. Usberti 7/a, 43100 Parma, Italy*
[3]*Department of Physics, University of Helsinki, Gustaf Hllstrmin katu 2a, P.O. Box 64, 00014 Helsinki, Finland*
[4]*Synchrotron SOLEIL, Orme des Merisiers, Saint-Aubin, B.P. 48, 91192 Gif-sur-Yvette Cedex, France*
(Received 13 October 2016; published 5 June 2017)

We present a detailed NMR study of the insulator-to-metal transition induced by an applied pressure p in the $A15$ phase of Cs_3C_{60}. We evidence that the insulating antiferromagnetic (AFM) and superconducting (SC) phases coexist only in a narrow p range. At fixed p, in the metallic state above the SC transition T_c, the ^{133}Cs and ^{13}C NMR spin-lattice relaxation data are seemingly governed by a pseudogaplike feature. We prove that this feature, also seen in the ^{133}Cs NMR shift data, is rather a signature of the Mott transition which broadens and smears out progressively for increasing (p, T). The analysis of the variation of the quadrupole splitting ν_Q of the ^{133}Cs NMR spectrum precludes any cell symmetry change at the Mott transition and only monitors a weak variation of the lattice parameter. These results open an opportunity to consider theoretically the Mott transition in a multiorbital three-dimensional system well beyond its critical point.

DOI: 10.1103/PhysRevLett.118.237601

In the cuprates, a Mott antiferromagnetic (AFM) insulating state is driven into a superconducting (SC) state by a chemically induced increase of the carrier content. Another paradigm for correlated electron systems is to induce such a change of electronic state by an applied pressure p [1,2]. An experimental realization requires a material with a large on-site Coulomb repulsion U to stabilize an insulating state at ambient p. A significant compressibility is then required to permit an increase with p of the bandwidth W, allowing one to span a large range of U/W values. Because of these restrictions, only a few compounds exhibit such an ideal Mott transition.

The most investigated compounds so far have been the vanadium oxides which exhibit a metal-to-insulator transition (MIT) above room T, though towards non-SC ground states. As for many other cases studied, a change in the atomic structure often occurs at the MIT, as, for instance, in doped VO_2, which displays a spin-Peierls transition concomitant to the MIT [3]. On the contrary, V_2O_3 undergoes a MIT [4,5], which has been considered as a prototypical case since the 1960s. It has been mostly studied in samples with slight Cr or Ti substitution on the V site that induces doping but also an uncontrolled amount of disorder. This yields an inhomogeneous phase coexistence range near the MIT [6].

Recently, original Mott transitions towards a SC ground state have been revealed in organic materials either of the bis(ethylenedithio)tetrathiafulvalene (BEDT-TTF) family [7,8] or in the fulleride compound Cs_3C_{60} [9,10]. Such compounds are highly compressible, as the bindings between the organic or fullerene molecules occur through van der Waals interactions. In the case of Cs_3C_{60}, detailed studies of the electronic properties have been limited, as actual samples are air-sensitive powders, often multiphased. However, NMR experiments permitted one to establish that a MIT occurs in both isomeric cubic forms of this compound. The $A15$ phase exhibits a transition from a Néel AFM to a SC metal with increasing p, while the fcc phase evolves from a frustrated magnetic state to a SC state [10,11]. Recent low-T experiments on a well-controlled nearly $A15$-pure sample permitted us [12] a thorough study of the SC state properties on the high-p side of the Mott transition.

On this improved sample, we evidence here that the AFM-SC phase coexistence range at the Mott transition is rather small. We furthermore show that at fixed p the thermal lattice expansion drives a transition between paramagnetic metal (PM) and insulating (PI) states, as reported for the organic conductor [8] and as was suggested [13] for the fulleride compound Na_2CsC_{60}. From NMR data taken on multiphased samples, we did initially suggest that such a transition occurs as well in the fcc Cs_3C_{60} [14]. Here the much higher experimental accuracy permits us to reveal the absence of a pseudogap, which differentiates the fullerides from the cuprates near their respective Mott transitions.

We further demonstrate that, at variance with the organic compounds, the slope dp/dT of the MIT remains positive over the whole phase diagram. Finally, the ^{133}Cs NMR quadrupolar splitting ν_Q reveals only a small step variation of the lattice parameter at the Mott transition. The increase at high pressure of the apparent width of the transition suggests a possible location of the critical point p_c in the phase diagram and allows us to compare the continuation of the Mott transition to a Widom line [15–17]. These results should also allow one to consider theoretically the incidence of

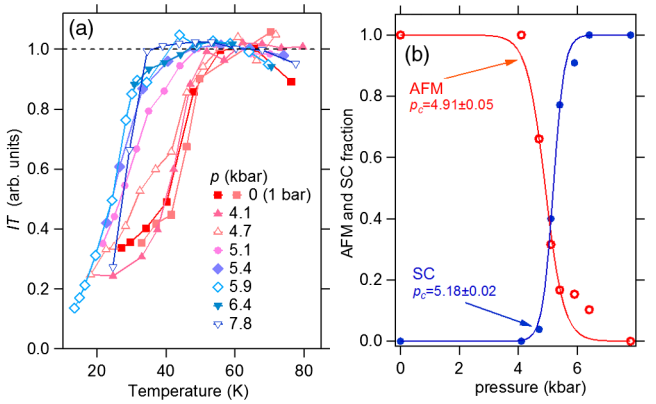

FIG. 1. (a) The ^{133}Cs NMR intensity corrected for its Curie $1/T$ dependence in the spectral range delineated in Fig. S1(a) of Ref. [21]. For any p, the intensity loss due to the AFM contribution is seen to onset below 50 K. (b) AFM fraction obtained by integrating the intensity between 50 and 35 K. Comparison with the SC fractions obtained in Ref. [12] from diamagnetic data.

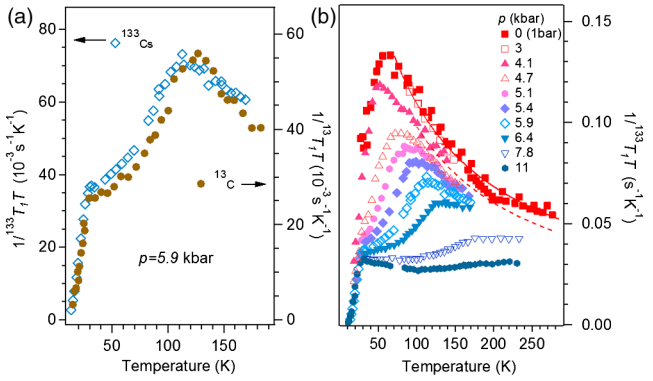

FIG. 2. (a) $(T_1T)^{-1}$ for ^{13}C and ^{133}Cs taken at 5.9 kbar with the vertical axes scaled. (b) The $^{133}(T_1T)^{-1}$ data are plotted versus T for a series of pressures p. The Curie-Weiss fits for 1 bar and 4.1 kbar (see the text) are plotted as solid and dotted lines, respectively. The step associated with the MIT shifts towards higher T with increasing p.

multiorbital [18] and Jahn-Teller [19,20] effects detected in these compounds.

Mott transition and low-T AFM-SC coexistence.—We present here a detailed investigation of the T variation of the ^{133}Cs NMR spectra at low p in the pure Mott-AFM phase and for $p > p_{c0} \sim 5$ kbar for which the SC state is fully established [12]. The ^{133}Cs NMR spectra exhibit a similar quadrupole splitting (for $I = 7/2$) in both paramagnetic regimes, but their shifts and width differ in the AFM and SC states (see [21], Sec. I). This permitted us to evaluate at a given p the AFM phase content from the signal loss occurring in the AFM state in a specific frequency window of the NMR spectrum, as detailed in Sec. I of Ref. [21]. As displayed in Fig. 1(a), the loss onsets below $T_N \sim 47$ K for all pressures $p < 5.4$ kbar, while it onsets only at $T_c \sim 35$ K for $p \geq 5.9$ kbar. Therefore, the magnetic and metallic states coexist only on a narrow p range with a quasiconstant Néel temperature. The comparison of the *local* NMR data on the magnetic state with the SC fraction taken on the *macroscopic* diamagnetic data is displayed in Fig. 1(b). It establishes that, up to $T = 50$ K, the transition occurs at the nearly T-independent pressure $p_{c0} = 5.1 \pm 0.3$ kbar. The sharpness of this transition with a small p extension $\Delta p/p_c = \pm 6\%$ of the coexistence regime is good evidence for the expected first-order character of the Mott transition.

Pseudogaplike variation of the NMR spin-lattice relaxation T_1 in the metallic state.—To follow the evolution of the electronic properties toward high T in the metallic state, we have first taken T_1 data on both ^{13}C and ^{133}Cs for a chosen pressure of 5.9 kbar, for which the sample is fully in the metallic state at low T. In the paramagnetic state, the nuclear magnetization recovery was found to exhibit a stretched exponential behavior $M(t)/M_0 = \exp[-(t/T_1)^{\beta}]$, with an identical exponent value $\beta = 0.85(5)$ (β did only slightly vary below T_N and T_c [12]). The large decrease of $(T_1T)^{-1}$ due to the opening of the SC gap is clearly evidenced in Fig. 2(a). There, one can see as well a large steplike increase for $T > 80$ K which is found to scale quite well for the two nuclear spin species. Being here very near to the Mott transition, one might consider that, in analogy to the case of underdoped cuprates, an incomplete pseudogap [27] opens and is followed by a full SC gap opening at lower T. However, for a wave-vector-dependent pseudogap due to AFM fluctuations, distinct T dependences of T_1 should occur for the two nuclear spin species, as ^{13}C resides on the magnetic C_{60} molecules (cf. ^{63}Cu in cuprates [28,29]), while ^{133}Cs, being located in a symmetric position in the AFM lattice, would hardly sense the AFM fluctuations (cf. ^{89}Y or ^{17}O in cuprates [27]).

Recovery of the insulating state at high T.—Such a pseudogap being ruled out by these data, we shall see hereafter that ^{133}Cs T_1 and NMR shift data for a series of pressures above and below p_{c0} do allow us to establish that the high-T transition corresponds to the restoration of a PI state.

(i) Paramagnetic state spin-lattice relaxation.—In Fig. 2(b), we report first former 1 bar data [10] taken on a large T range on distinct samples sealed in glass capillaries. There we recognize the large increase of $(T_1T)^{-1}$ with decreasing T [10,11], followed by a sharp decrease due to the opening of the magnetic gap in the AFM state below $T_N = 47$ K. In the PI state, this variation corresponds to a Curie-Weiss-like behavior $(T_1T)^{-1} = B/(T + \theta)$ with $\theta = 60 \pm 5$ K, of the order of magnitude of T_N as expected for a dense paramagnet [10,11]. In Fig. 2(b), we report then a series of $(T_1T)^{-1}$ data for $p > 2$ kbar taken on the sample housed in the pressure cell. Below 4.7 kbar, they exhibit convex T dependences similar to that seen on the 1 bar samples. The small 20% magnitude deviation could be mainly assigned to sample and NMR

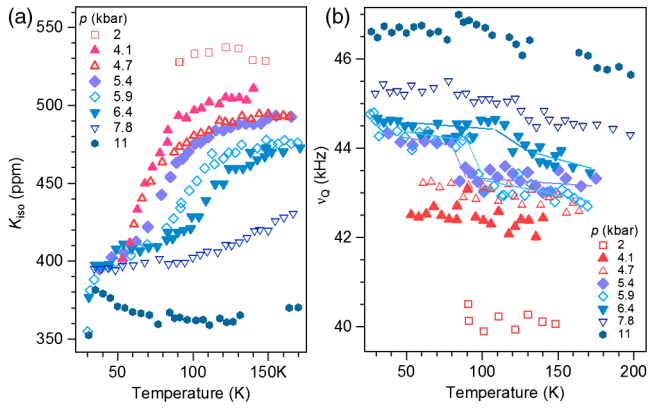

FIG. 3. The ^{133}Cs NMR spectral analyses done in Sec. II of Ref. [21] yield (a) $K_{\rm iso}$ on a large (T, p) range which displays step variations for increasing T similar to those found for $(T_1T)^{-1}$ in Fig. 2(b) and (b) ν_Q data do reveal small jumps of ~1 kHz for $5.4 < p < 6.4$ kbar which disappear at higher p. Lines are guides to the eye.

probe differences in the two experimental setups. For all pressures $p > 5.1$ kbar, we see that the formerly studied [12] SC state increase of $(T_1T)^{-1}$ up to T_c is followed by a second steplike increase as that seen in Fig. 2(a). This is evidenced by the inflection point and the concave variation displayed by all the data curves. One might notice that, at higher T values, $(T_1T)^{-1}$ recovers a decreasing behavior strikingly identical to that seen for the PI state at 4.1 kbar. This ascertains that the step increase of $(T_1T)^{-1}$ indeed locates the MIT. For $p \geq 7.8$ kbar, an intermediate plateau of $(T_1T)^{-1}$ suggestive of a PM Korringa behavior [30] can be noticed between the two regimes.

(ii) NMR shifts from the ^{133}Cs NMR spectra.—The transition from a PM to a PI can be detected as well on the electronic spin susceptibility, which can be monitored from the ^{133}Cs NMR shift. With a single $I = 7/2$ Cs nuclear spin site, the spectra could be fitted as exemplified in Sec. II of Ref. [21] to deduce the NMR shift tensor, the quadrupole frequency ν_Q, and its asymmetry parameter η. For all pressures below 11 kbar, the isotropic contribution $K_{\rm iso}$ to the NMR shift increases with T as shown in Fig. 3(a). In the PI range, this increase above T_N is due to the progressive decorrelation of the local moments. For $p \gtrsim 5.9$ kbar, the recovery of the NMR shift at $T_c \gtrsim 30$ K is followed by a steplike increase of $K_{\rm iso}$ quite identical to that seen for the $(T_1T)^{-1}$ data. One can even see in Ref. [21] that $(T_1T)^{-1}$ linearly scales with $K_{\rm iso}$ in the intermediate T range where the two quantities increase sharply. These results allow us to establish unambiguously that the transition $T_{\rm MIT}(p)$ from the PM to the PI state shifts towards higher T for increasing p.

Structural changes at the transition.—Former synchrotron radiation x-ray data taken on a very large p range permitted one to detect only an overall variation of the lattice parameter [9]. We also took x-ray data, described in Sec. III of Ref. [21], which allows us to confirm that the $A15$ lattice cell symmetry is not subsequently modified from the Mott state up to $p = 11$ kbar. The nuclear quadrupole frequency ν_Q deduced from the ^{133}Cs NMR spectra is also directly related to the distribution of charges and then to the atomic structure and the ordering of the C_{60} molecular orbitals. The extensive spectral fits described in Ref. [21] permitted us to determine the T variations of ν_Q shown in Fig. 3(b). Those are naturally found quite smooth in the absence of any crossing of the MIT for $p < 4.7$ kbar. However, for $5.1 < p < 7$ kbar, minute step decreases of ν_Q with increasing T are evidenced near the transition temperatures detected from the T_1 and $K_{\rm iso}$ data of Figs. 2(b) and 3(a). No such signature of the transition could be detected at higher p. We recall that ν_Q gives a measure of the electric field gradient (EFG) on the Cs atomic site with $\nu_Q \propto d^2V/dr^2$, where $V(r)$ is the potential around the Cs site located at $r = 0$. As $V(r)$ has dimension L^{-1}, ν_Q has dimension L^{-3}. Assuming a uniform lattice contraction with increasing p, this dimensional analysis demonstrates that one roughly expects $\nu_Q \propto a^{-3} = 1/v$, where v is the lattice unit cell volume. We shall consider first the qualitative information gained on the phase diagram from the ν_Q data, while a quantitative analysis of the variation of lattice parameter will be attempted later.

Phase diagram.—The data presented above permitted us to evidence on $(T_1T)^{-1}$, $K_{\rm iso}$, and ν_Q that the metallic state crosses over toward the insulating state with increasing T at a given p. We are now able to discuss the main characteristics of the transition line $T_{\rm MIT}(p)$ and its apparent width.

(i) Transition line.—We already know from the discussion done on the AFM-SC fractions that the transition line is nearly vertical at $p = 5.1$ kbar, from $T = 0$ to 50 K. For higher p, the temperature T_Q at which a small step decrease of ν_Q is detected permits one to locate the evolution of the transition up to $p \sim 6.4$ kbar. The magnetic responses $(T_1T)^{-1}$ and $K_{\rm iso}$, which scale with each other in the metallic regime (see [21], Sec. II), give a determination of the transition which can be followed at larger p. The maximum of $(T_1T)^{-1}$ marks the full restoration of the insulating state that is the upper limit $T_{\rm max}$ for the MIT. One might as well assign a width to the transition and consider that the MIT sits at the inflection point $T_{{\rm mid}(T_1)}$ of $(T_1T)^{-1}$ versus T (or equivalently $T_{{\rm mid}(K)}$ for $K_{\rm iso}$ versus T), which can be obtained by fitting the fixed p data with a steplike function with a half intensity width Δ_T, as done in Sec. II of Ref. [21]. The data for $T_{\rm max}$, T_Q, $T_{{\rm mid}(T_1)}$, and $T_{{\rm mid}(K)}$ plotted in Fig. 4 give therefore a good representation of the variation of the MIT, which bends over for increasing p in the actual phase diagram. In the fcc Cs_3C_{60} phase, a similar MIT transition line has been suggested solely from NMR T_1 data taken with increasing pressure (Figs. 5 and 6 of Ref. [14]) or for Rb-substituted samples [20].

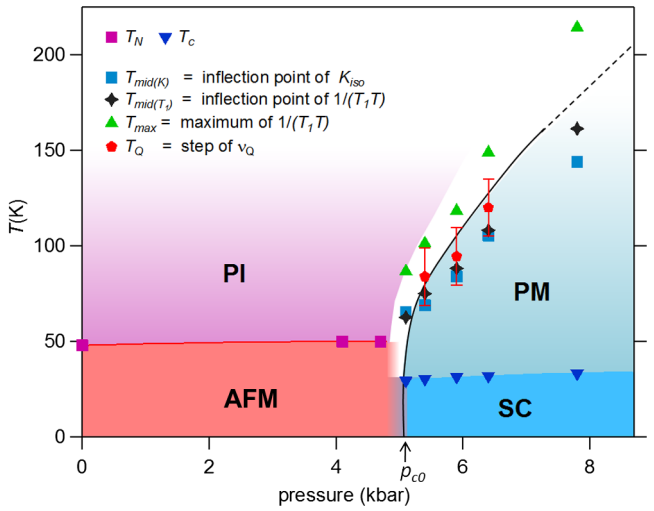

FIG. 4. MIT transition temperatures T_Q, $T_{\mathrm{mid}(T_1)}$, $T_{\mathrm{mid}(K)}$, and $T_{\max}$ deduced from ^{133}Cs NMR data for $p > 5.4$ kbar. The T_Q data mark the weak first-order regime (solid line), while $T_{\max}$ delineates the apparent upper half width of the transition given as the blank zone. This suggests that the transition becomes a crossover (dotted line) at high (T, p) beyond a critical point $p_c \simeq 7$ kbar (see the text). The AFM and SC fractions measured in Fig. 1(b) yielded $p_{c0} = 5.1 \pm 0.3$ kbar below 35 K. The phase diagram is completed by the horizontal T_N line below 5.1 kbar, and the T_c dome above 5.1 kbar.

(ii) Transition width and critical point.—We may anticipate that, in the absence of sample defects and of p distribution in the pressure cell, the transition should be much narrower and display the hysteresis expected for a first-order transition, as found in organics [8]. If due to a purely inhomogeneous broadening, the 0.3 kbar half width of the transition determined for $p \simeq 5$ kbar in Fig. 1 should increase linearly up to 0.5 kbar for $p = 7.8$ kbar. From the 30 K/kbar slope of $T_{\mathrm{MIT}}(p)$ of Fig. 4, one would expect at most $\Delta_T = 15$ K, obviously much smaller than $\Delta_T = 50$ K obtained experimentally at 7.8 kbar (see [21], Sec. II). Therefore, the large increase of Δ_T at high p is apparently governed by a fundamental intrinsic effect. This behavior is indicative of a suppression of the first-order transition above a critical pressure p_c. The latter can be tentatively located at $\simeq$7 kbar, as the transition cannot be detected on ν_Q data between 6.4 and 7.8 kbar. Therefore, beyond p_c the transition line is rather the loci of a continuation of the first-order transition usually considered as a Widom line [15–17]. Its location is well known to depend somewhat on the thermodynamic quantity employed, even for classical systems such as the liquid-gas transition.

Discussion of ν_Q.—Let us consider the physical significance of the p and T variations of ν_Q on the Cs site. As discussed above, for a uniform contraction of the unit cell in a simple point charge model, one expects $d\nu_Q/\nu_Q = -dv/v$. The x-ray data (see [21], Sec. III) taken at $T = 14.5$ K correspond to an initial linear p dependence of the lattice cell volume $dv/(vdp) = -6.2 \times 10^{-3}$/kbar. From Fig. 3(b), we obtain $d\nu_Q/\nu_Q dp = 0.02$/kbar for $p < 5$ kbar at a fixed T of 50 (or 80) K for which the sample remains in the PI state. Therefore, ν_Q exhibits a 3 times faster increase with unit cell contraction than expected. While this limits the significance of the model, we may consider that this experimental scaling can be applied as well for the $\simeq$1 kHz decrease of ν_Q at the MIT. That would correspond to about $\delta v/v \simeq 0.008$, that is, an increase of lattice parameter $da/a \simeq 2 \times 10^{-3}$, which is within the error bar of the synchrotron x-ray data we have collected so far in diamond anvil cells [21].

Let us recall here that ν_Q involves two contributions $\nu_Q = \nu_{Q,i} + \nu_{Q,b}$. The first one, associated with the EFG created by large distance ions, is correctly estimated within the above model. The second contribution is due to the ionic charges and electrons distributed in the Cs first-nearest neighbor molecular C_{60} orbitals. In the absence of a modification of the C_{60} ball diameter with p and T (confirmed in Ref. [21], Sec. III), the unit cell does not contract uniformly. This might essentially control the local contribution $\nu_{Q,b}$ associated with the C_{60} molecular orbitals, which could as well be sensitive to the appearance of extended states at the Mott transition.

Conclusion.—We have shown here that $A15$ Cs_3C_{60} presents a quasi-ideal Mott transition and performed an NMR study which allowed us to reveal the absence of a pseudogap and charge order near the Mott transition. This lack of competing order might explain that T_c remains quite high up to the MIT, conversely to the case of hole-doped cuprates. We could establish altogether the evolution of the MIT first-order line in the (p, T) phase diagram towards a continuous transition. Quite remarkably, we also find that the insulating state restored from the metallic state by the thermal expansion of the lattice has magnetic properties quite analogous to those found at high T in the pure insulating Mott state. This might indicate that quantum fluctuations do govern the continuous transition at high (p, T), which therefore differs from the Widom line occurring in classical systems, e.g., the liquid-gas transition. Let us recall as well that the maximum of $(T_1T)^{-1}$ versus T, which has been revealed for some time [31], in the dense A_3C_{60} light-alkali compounds is quite similar to that detected here above $p = 7.8$ kbar. This gives a strong hint that in all these compounds the maximum of $(T_1T)^{-1}$ represents the crossover towards the local moment behavior of the PI state. Finally, contrary to the case of the organic triangular lattice crystals, the critical line has a positive slope with respect to p. This entropy-related slope, which suggests higher entropy in the insulating state linked with orbital degeneracy, qualitatively agrees with the results of dynamical mean field theory (DMFT) calculations for fcc A_3C_{60} (A = K, Rb, Cs) [18]. More quantitative simulations taking into account the $A15$ A_3C_{60} lattice geometry could

permit one to investigate the interplay between orbital and spin degrees of freedom in this genuine Mott transition.

We acknowledge Synchrotron-SOLEIL for providing beam time and thank S. Ravy for assistance in taking x-ray data on the CRISTAL beam line (Projects No. 2010286 and No. 20110678). We also have had stimulating discussions with S. Biermann, Y. Nomura, V. Dobrosavlevic, and M. Rozenberg.

[1] N. Mott, Rev. Mod. Phys. **40**, 677 (1968).
[2] N. Mott, *Metal-Insulator Transitions* (Taylor & Francis, London, 1990).
[3] J. P. Pouget, H. Launois, J. P. D'Haenens, P. Merenda, and T. M. Rice, Phys. Rev. Lett. **35**, 873 (1975).
[4] D. B. McWhan and T. M. Rice, Phys. Rev. Lett. **22**, 887 (1969).
[5] D. B. McWhan, T. M. Rice, and J. P. Remeika, Phys. Rev. Lett. **23**, 1384 (1969).
[6] I. Leonov, V. I. Anisimov, and D. Vollhardt, Phys. Rev. B **91**, 195115 (2015).
[7] S. Lefebvre, P. Wzietek, S. Brown, C. Bourbonnais, D. Jérome, C. Mézière, M. Fourmigué, and P. Batail, Phys. Rev. Lett. **85**, 5420 (2000).
[8] F. Kagawa, K. Miyagawa, and K. Kanoda, Nature (London) **436**, 534 (2005).
[9] Y. Takabayashi, A. Y. Ganin, P. Jeglic, D. Arcon, T. Takano, Y. Iwasa, Y. Ohishi, M. Takata, N. Takeshita, K. Prassides, and M. J. Rosseinsky, Science **323**, 1585 (2009).
[10] Y. Ihara, H. Alloul, P. Wzietek, D. Pontiroli, M. Mazzani, and M. Riccò, Phys. Rev. Lett. **104**, 256402 (2010).
[11] P. Jeglič, D. Arčon, A. Potočnik, A. Y. Ganin, Y. Takabayashi, M. J. Rosseinsky, and K. Prassides, Phys. Rev. B **80**, 195424 (2009).
[12] P. Wzietek, T. Mito, H. Alloul, D. Pontiroli, M. Aramini, and M. Riccò, Phys. Rev. Lett. **112**, 066401 (2014).
[13] V. Brouet, H. Alloul, S. Garaj, and L. Forró, Phys. Rev. B **66**, 155122 (2002).
[14] Y. Ihara, H. Alloul, P. Wzietek, D. Pontiroli, M. Mazzani, and M. Riccó, Europhys. Lett. **94**, 37007 (2011).
[15] V. V. Brazhkin, Y. D. Fomin, A. G. Lyapin, V. N. Ryzhov, and E. N. Tsiok, J. Phys. Chem. B **115**, 14112 (2011).
[16] L. Xu, P. Kumar, S. Buldyrev, S. Chen, P. Poole, F. Sciortino, and H. Stanley, Proc. Natl. Acad. Sci. U.S.A. **102**, 16558 (2005).
[17] J. Luo, L. Xu, E. Lascaris, H. E. Stanley, and S. V. Buldyrev, Phys. Rev. Lett. **112**, 135701 (2014).
[18] Y. Nomura, S. Sakai, M. Capone, and R. Arita, J. Phys. Condens. Matter **28**, 153001 (2016).
[19] G. Klupp, P. Matus, K. Kamarás, A. McLennan, M. Rosseinsky, Y. Takabayashi, M. McDonald, and K. Prassides, Nat. Commun. **3**, 912 (2012).
[20] R. H. Zadik, Y. Takabayashi, G. Klupp, R. H. Colman, A. Y. Ganin, A. Potočnik, P. Jeglič, D. Arčon, P. Matus, K. Kamarás, Y. Kasahara, Y. Iwasa, A. N. Fitch, Y. Ohishi, G. Garbarino, K. Kato, M. J. Rosseinsky, and K. Prassides, Sci. Adv. **1**, e1500059 (2015).
[21] See Supplemental Material at http://link.aps.org/supplemental/10.1103/PhysRevLett.118.237601, which includes Refs. [22–26], for the analysis of the AFM fraction near the MIT from the ^{133}Cs NMR spectra, in section I. The quadrupole frequency ν_Q and the NMR shift data in the paramagnetic state are deduced from the detailed spectral fits of the ^{133}Cs NMR spectra in section II. The latter are compared with the $(T_1T)^{-1}$ data. In section III the x-ray spectra for three different pressures are reported and the deduced temperature variations of the lattice parameter are discussed.
[22] Multiparameter fits of the NMR spectra were done using the genetic optimization algorithm described in A. Nelson, J. Appl. Crystallogr. **39**, 273 (2006).
[23] G. J. Piermarini, S. Block, J. D. Barnett, and R. A. Forman, J. Appl. Phys. **46**, 2774 (1975).
[24] A. Y. Ganin, Y. Takabayashi, Y. Z. Khimyak, S. Margadonna, A. Tamai, M. J. Rosseinsky, and K. Prassides, Nat. Mater. **7**, 367 (2008).
[25] S. Fujiki, Y. Kubozono, M. Kobayashi, T. Kambe, Y. Rikiishi, S. Kashino, K. Ishii, H. Suematsu, and A. Fujiwara, Phys. Rev. B **65**, 235425 (2002).
[26] G. J. Burkhart and C. Meingast, Phys. Rev. B **54**, R6865 (1996).
[27] H. Alloul, T. Ohno, and P. Mendels, Phys. Rev. Lett. **63**, 1700 (1989).
[28] R. Walstedt, *The NMR Probe of High Tc Materials*, Springer Tracts in Modern Physics Vol. 228 (Springer, Berlin, 2008).
[29] M. Takigawa, A. P. Reyes, P. C. Hammel, J. D. Thompson, R. H. Heffner, Z. Fisk, and K. C. Ott, Phys. Rev. B **43**, 247 (1991).
[30] A. Abragam, *The Principles of Nuclear Magnetism* (Clarendon, Oxford, 1973).
[31] K. Holczer, O. Klein, H. Alloul, Y. Yoshinari, F. Hippert, S.-M. Huang, R. B. Kaner, and R. L. Whetten, Europhys. Lett. **23**, 63 (1993).